

Supporting Information

A magnetically separable and recyclable g -C₃N₄/Fe₃O₄/porous ruthenium nanocatalyst for the photocatalytic degradation of water-soluble aromatic amines and azo-dyes

Anupam Sahoo and Srikanta Patra*

School of Basic Sciences. Indian Institute of Technology Bhubaneswar, Argul, Jatni-752050, Orissa, India
E-mail: srikanta@iitbbs.ac.in.

Table of content

Sr. No.	Description	Page No.
1	Chart S1. Chemical structure of aromatic amines used in this study.	S3
2	Chart S2. Chemical structure of azo dyes used in this study.	S4
	Table TS1. Comparison between the present and other related nanocatalysts towards removal of aromatic amines.	S5
3	Table TS2. Catalytic reduction of azo dyes in presence of $g\text{-C}_3\text{N}_4/\text{Fe}_3\text{O}_4/p\text{-RuNP}$ nanocomposites and NaBH_4 .	S7
4	Figure S1. FE-SEM images of (a) $g\text{-C}_3\text{N}_4$ nanosheet, (b) $g\text{-C}_3\text{N}_4/\text{Fe}_3\text{O}_4\text{NP}$ and (c) $g\text{-C}_3\text{N}_4/\text{Fe}_3\text{O}_4/p\text{-RuNP}$ nanocomposites and (d-f) their corresponding EDS spectra, respectively.	S8
5	Figure S2. SEM image (a) and mapping of (b) elemental C, (c) elemental N, (d) elemental O (e) elemental Fe and (f) elemental Ru of $g\text{-C}_3\text{N}_4/\text{Fe}_3\text{O}_4/p\text{-RuNP}$ nanocomposite.	S9
6	Figure S3. Powder XRD patterns of $g\text{-C}_3\text{N}_4$ nanosheet, $g\text{-C}_3\text{N}_4/\text{Fe}_3\text{O}_4\text{NP}$ and $g\text{-C}_3\text{N}_4/\text{Fe}_3\text{O}_4/p\text{-RuNP}$ nanocomposites.	S10
7	Figure S4. (a) N_2 adsorption-desorption isotherms and (b) pore size distribution of $g\text{-C}_3\text{N}_4$, $g\text{-C}_3\text{N}_4/\text{Fe}_3\text{O}_4\text{NP}$ and $g\text{-C}_3\text{N}_4/\text{Fe}_3\text{O}_4/p\text{-RuNP}$ nanocomposites.	S11
8	Figure S5. (a) UV-Vis DRS spectra and (b) Tauc plot of $g\text{-C}_3\text{N}_4$, $g\text{-C}_3\text{N}_4/\text{Fe}_3\text{O}_4\text{NP}$ and $g\text{-C}_3\text{N}_4/\text{Fe}_3\text{O}_4/p\text{-RuNP}$.	S12
9	Figure S6. Photocatalytic degradation of aniline (100 mg/L) by $g\text{-C}_3\text{N}_4/\text{Fe}_3\text{O}_4/p\text{-RuNP}$ at (a) different pH (b) with varying ruthenium concentration and (c) varying aniline concentration after 24 h under LED.	S13
10	Figure S7. UV-Vis spectra and HPLC of aromatic amines (100 mg/L) and after degradation using visible light at pH 7.0 in presence of $g\text{-C}_3\text{N}_4/\text{Fe}_3\text{O}_4/p\text{-RuNP}$ nanocatalyst (80 mg/L).	S14
11	Figure S8. Photograph of CR dye of varying concentration (a) before and (b) after photodegradation (1h) by $g\text{-C}_3\text{N}_4/\text{Fe}_3\text{O}_4/p\text{-RuNP}$ nanocomposite and (c) the corresponding UV-Vis spectra.	S15
12	Figure S9. UV-Vis spectra of degradation of various azo dyes (5 mg/L) under LED in presence of $g\text{-C}_3\text{N}_4/\text{Fe}_3\text{O}_4/p\text{-RuNP}$ nanocatalyst (80 mg/L).	S16
13	Figure S10. HPLC of azo-dyes (5 mg/L) after and before the degradation using visible light at pH 7.0 in presence of $g\text{-C}_3\text{N}_4/\text{Fe}_3\text{O}_4/p\text{-RuNP}$ (80 mg/L) nanocatalyst.	S17
14	Figure S11. FTIR spectra of CR, $g\text{-C}_3\text{N}_4/\text{Fe}_3\text{O}_4/p\text{-RuNP}$ nanocatalyst before and after photo-degradation of CR and the solution after complete degradation of CR.	S18
15	Figure S12. (a, c, e and g) UV-Vis spectra of azo dyes before (i), after(ii) reduction and after photo-degradation (iii); (b, d, f and h) HPLC of aromatic amines of reduced dyes (200 mg/L) after and before degradation using visible light at pH 7.0 in presence of $g\text{-C}_3\text{N}_4/\text{Fe}_3\text{O}_4/p\text{-RuNP}$ nanocatalyst (80 mg/L).	S19
16	Figure S13. Reusability of $g\text{-C}_3\text{N}_4/\text{Fe}_3\text{O}_4/p\text{-RuNP}$ nanocatalyst towards aniline (100 mg/L) degradation under visible (LED) light.	S20
17	Figure S14. (a) UV-Vis spectra of CR after treatment of $g\text{-C}_3\text{N}_4/\text{Fe}_3\text{O}_4/p\text{-RuNP}$ nanocatalyst in the presence of different radical scavengers under LED light.	S21
18	References	S22

Chart S1. Chemical structure of aromatic amines used in this study.

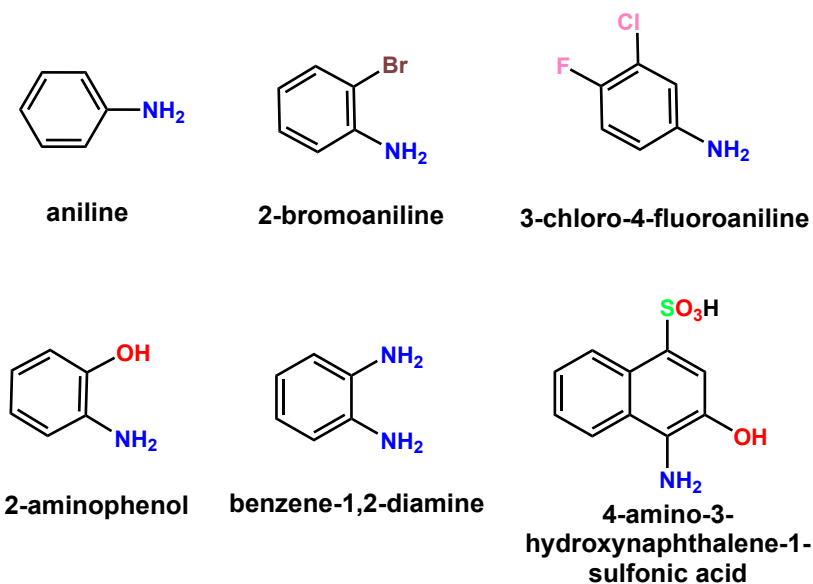


Chart S2. Chemical structure of azo dyes used in this study.

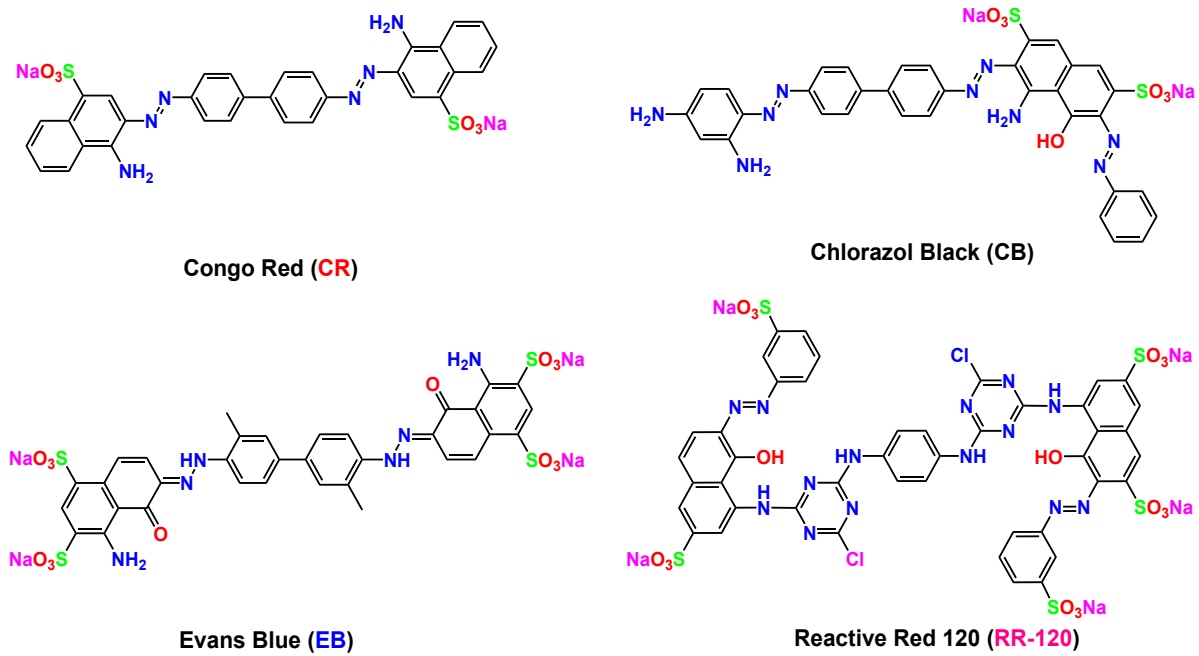


Table TS1. Comparison between the present and other related nanocatalysts towards removal of aromatic amines.

Sl. No.	Title	Name of the enzyme/chemical/catalyst	Aromatic amine/hydroxy compounds used	Initial conc. of Dye/Aromatic amines	Medium/Buffer/temp./pH	% removal
1	Chemical degradation of aromatic amines by Fenton's reagent ¹	Fenton's reagent [Fe(II) + H ₂ O ₂] (100-500 mg/L)	o-dianisidine, naphthylamine, 2-naphthylamine, 3,3'-dichlorobenzidine, p-anisidine, 4-chloroaniline, 2,4-iaminotoluene, o-tolidine and aniline.	1-2-3,3'-4-	0.0003 mM pH 4.5-5.5	100
2	Removal of aromatic amines and decolourisation of azo dye baths by electrochemical treatment ²	Electrochemical treatment 20 g of diatomaceous earth (90% SiO ₂)	aniline, o-toluidine, chloroaniline and aminobiphenyl	4-4-	300 mg/L Dye and 10mg/L Aromatic amines	90
3	Chemical coagulation and sonolysis for total aromatic amines removal from anaerobically pre-treated textile wastewater: A comparative study ³	Chemical coagulation, sonolysis Magnesium chloride aided with aluminium chlorohydrate (1800 mg /L)	Azo dyes (CR, RB 5, Disperse blue 3) Aromatic amine: Benzidine, sulfonic acid	200 mg/L	pH 7.0	85 (AAs) 52 (Decolorization of dyes)
4	Horseradish peroxidase for the removal of carcinogenic aromatic amines from water ⁴	Horseradish peroxidase (100U/L) and hydrogen peroxide(1M)	o-tolidine, and 2-naphthylamine; from Aldrich, 1-naphthylamine, 4-aminobiphenyl, pphenylazoaniline, aniline, p-toluidine	100mg/L	pH 5.0	99
5	Removal of direct azo dyes and aromatic amines from aqueous solutions using two - cyclodextrin-based polymers ⁵	b-Cyclodextrin (b-CD) (2.5 g/L)	benzidine, p-chloroaniline and -naphthalamine	0.001 mM	pH 7.0	>85
6	Removal efficiency of a calix[4]arene-based polymer for water-soluble carcinogenic direct azo dyes and aromatic amines ⁶	calix[4]arenes derivative (2.5 g/L)	Azo dyes and aromatic amines (benzidine, p-chloroaniline, -naphthalamine)	0.001 mM	pH 2.0	>90

7	A porous trimetallic Au@Pd@Ru nanoparticle system: synthesis, characterisation and efficient dye degradation and removal ⁷	Porous Au@Pd@Ru Dolochar(150g/L)	Benzidine,benzidine, aminophenol and dimethoxyaniline	4-3,4	Dye and Aromatic amines= 1mM	pH=7.0	>90
8	A Combined Process for the Degradation of Azo-Dyes and Efficient Removal of Aromatic Amines Using Porous Silicon Supported Porous Ruthenium Nanocatalyst ⁸	Porous silicon@porous ruthenium(8 mL in 1 L) and H ₂ O ₂ (1M) (amount of Ru ≈ 3.39 ppm)	Azo dyes and aromatic amines	Dye and Aromatic amines= 1mM	pH=5.0	46-99	
9	A magnetically separable and recyclable porous Ruthenium nanocatalyst for the photocatalytic degradation of water-soluble aromatic amines and azo-dyes ^{Present Work}	80 mg/L 100 W, visible LED light (amount of Ru ≈ 3.44 ppm)	Azo dyes and aromatic amines	Dye(200mg /L) Aromatic amines (100-200mg/L)	pH 7.0	The percentage varies from 67-99 And the catalyst is recyclable several times	

Table TS2. Catalytic reduction of azo dyes in presence of g -C₃N₄/Fe₃O₄/*p*-RuNP nanocomposites and NaBH₄.

Sr. No	Name of the dye/amine	Concentration	Catalyst (per 10 mL)	Time of reaction	Removal efficiency
1	CR	5 mg/L	200 μ L	1 h	100 %
2	CB	5 mg/L	200 μ L	1 h	100 %
3	EB	5 mg/L	200 μ L	18 h	100%
4	RR-120	5 mg/L	200 μ L	2 h	98%

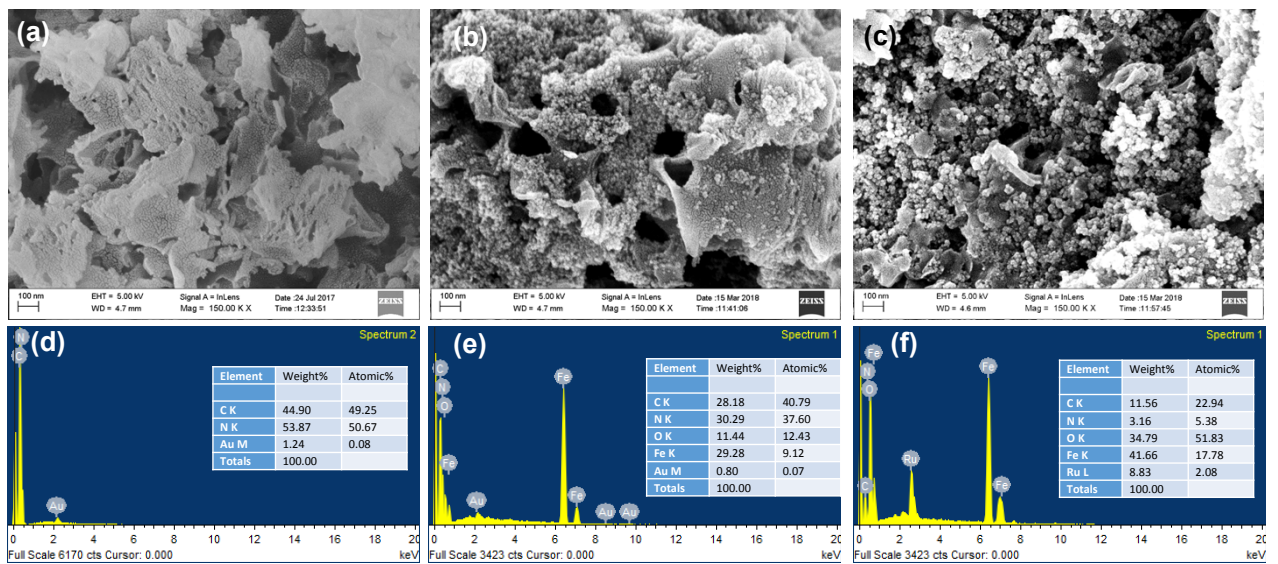


Figure S1. FE-SEM images of (a) $g\text{-C}_3\text{N}_4$ nanosheet, (b) $g\text{-C}_3\text{N}_4/\text{Fe}_3\text{O}_4\text{NP}$ and (c) $g\text{-C}_3\text{N}_4/\text{Fe}_3\text{O}_4/p\text{-RuNP}$ nanocomposites and (d-f) their corresponding EDS spectra, respectively.

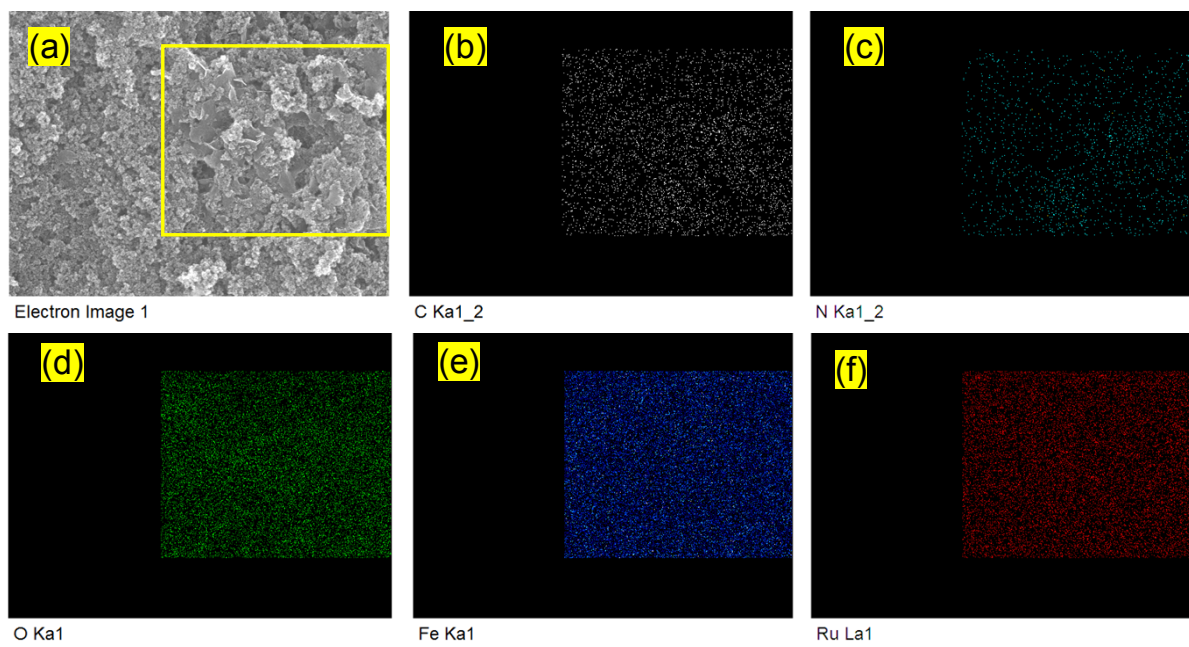


Figure S2. SEM image (a) and mapping of (b) elemental C, (c) elemental N, (d) elemental O (e) elemental Fe and (f) elemental Ru of $g\text{-C}_3\text{N}_4/\text{Fe}_3\text{O}_4/p\text{-RuNP}$ nanocomposite.

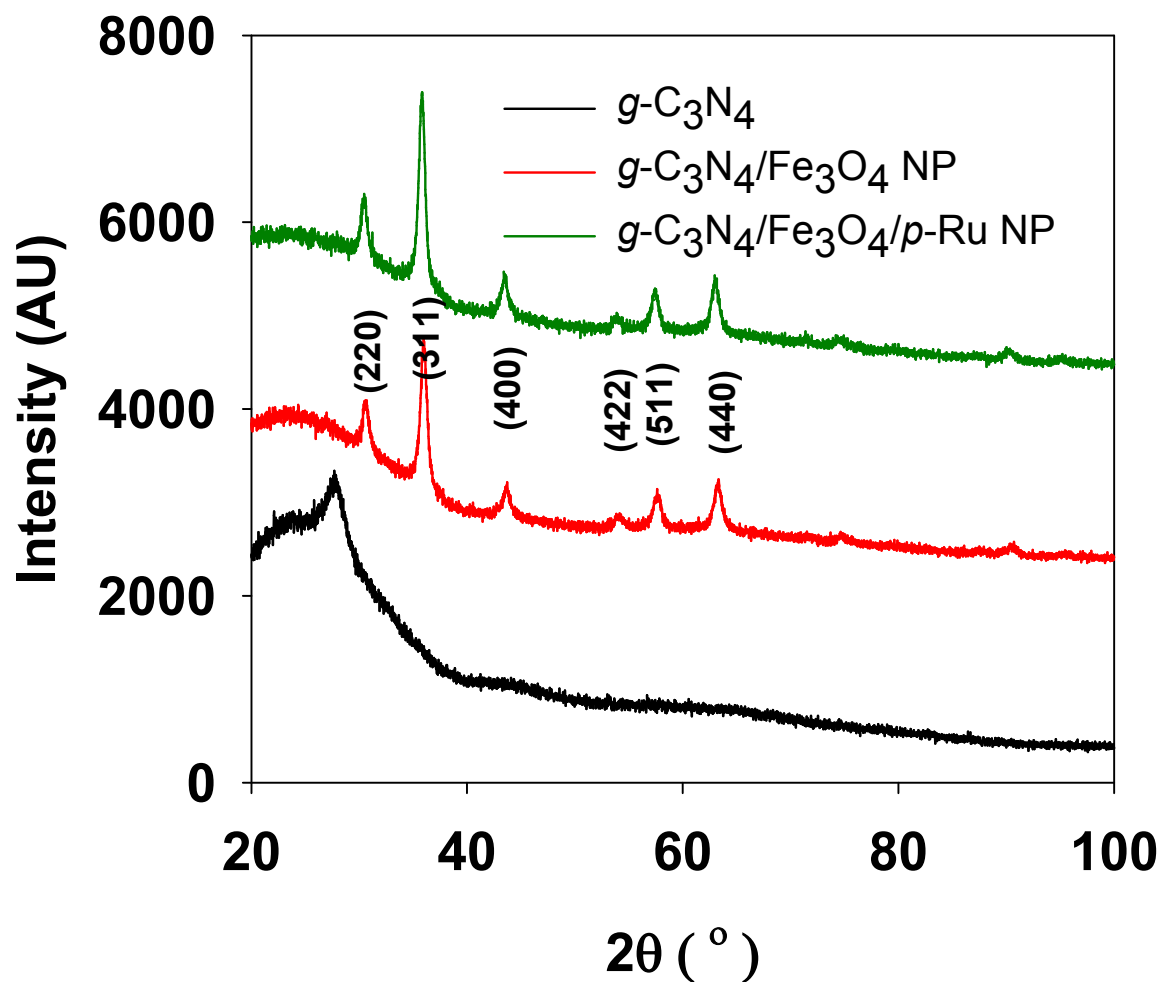


Figure S3. Powder XRD patterns of $g\text{-C}_3\text{N}_4$ nanosheet, $g\text{-C}_3\text{N}_4/\text{Fe}_3\text{O}_4$ NP and $g\text{-C}_3\text{N}_4/\text{Fe}_3\text{O}_4/p\text{-Ru}$ NP nanocomposites.

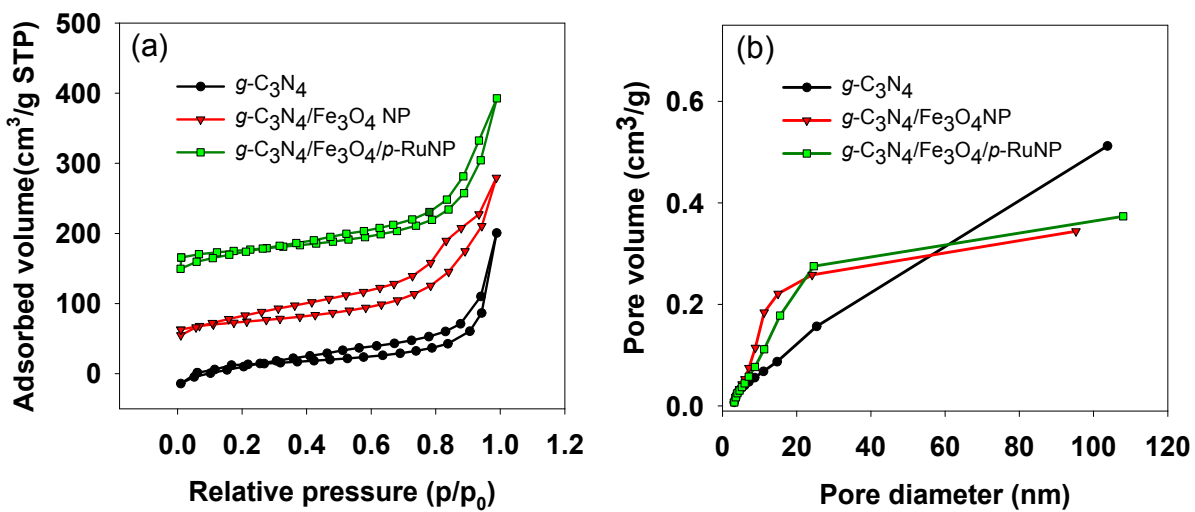


Figure S4. (a) N₂ adsorption-desorption isotherms and (b) pore size distribution of g-C₃N₄, g-C₃N₄/Fe₃O₄NP and g-C₃N₄/Fe₃O₄/p-RuNP nanocomposites.

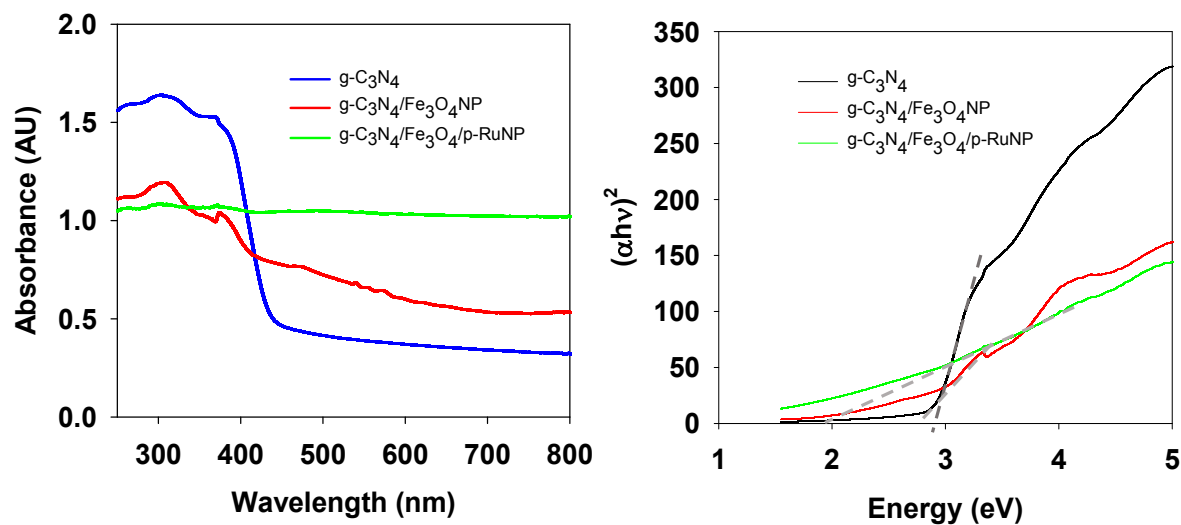


Fig. S5. (a) UV-Vis DRS spectra and (b) Tauc plot of $g\text{-C}_3\text{N}_4$, $g\text{-C}_3\text{N}_4/\text{Fe}_3\text{O}_4\text{NP}$ and $g\text{-C}_3\text{N}_4/\text{Fe}_3\text{O}_4/p\text{-RuNP}$.

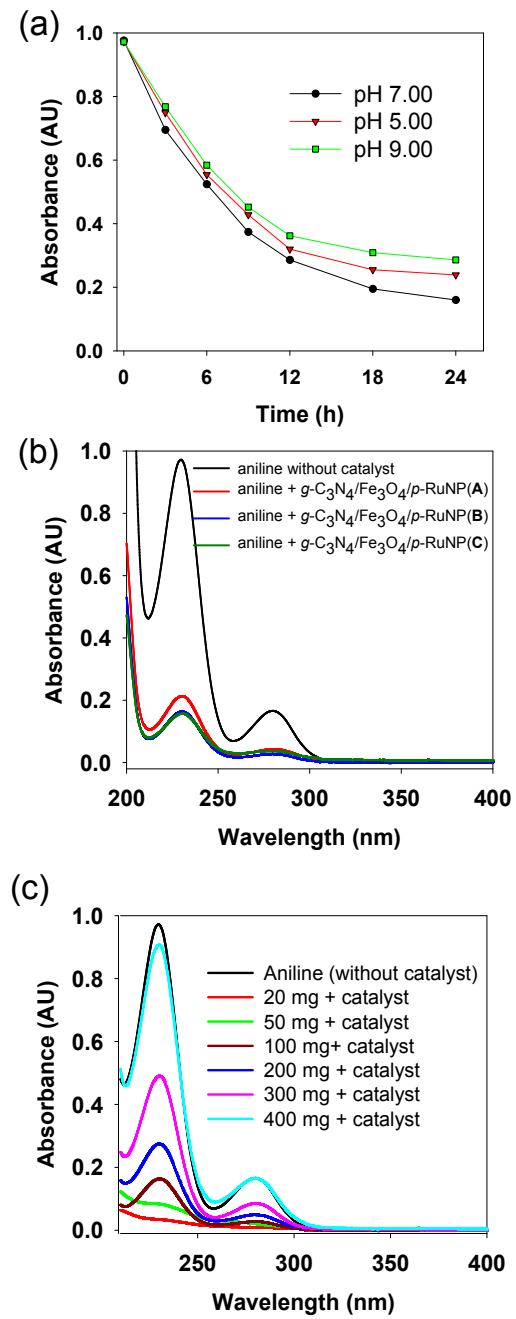


Figure S6. Photocatalytic degradation of aniline (100 mg/L) by $g\text{-C}_3\text{N}_4/\text{Fe}_3\text{O}_4/p\text{-RuNP}$ at (a) different pH (b) with varying ruthenium concentration and (c) varying aniline concentration after 24 h under LED.

* catalysts were taken 80 mg containing 3.44 ppm of Ru^0 ; The catalysts **A**, **B** and **C** were prepared by taking 5 mM, 10 mM and 20 mM $\text{RuCl}_3 \cdot \text{nH}_2\text{O}$.

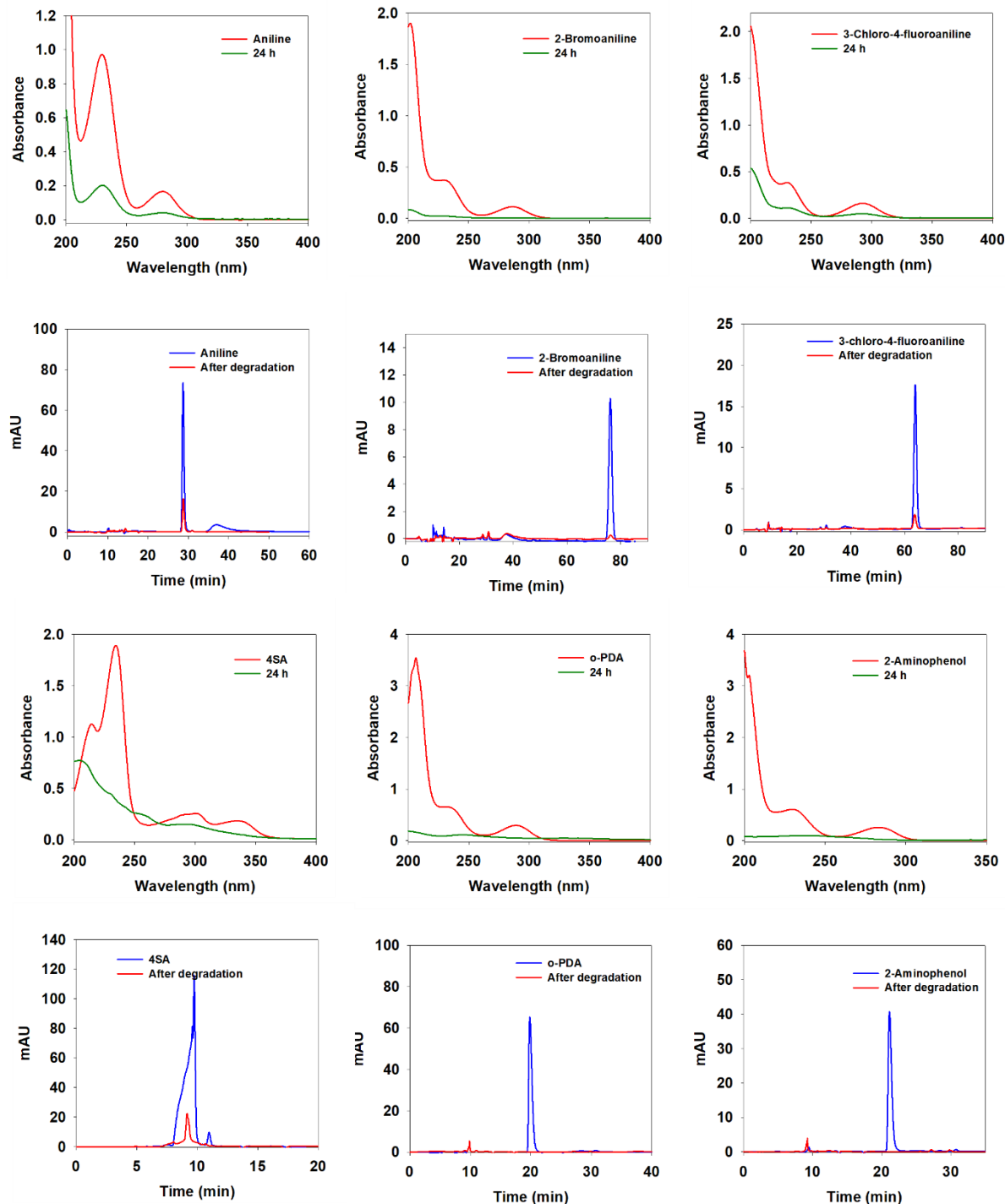


Figure S7. UV-Vis spectra and HPLC of aromatic amines (100 mg/L) and after degradation using visible light at pH 7.0 in presence of $g\text{-C}_3\text{N}_4/\text{Fe}_3\text{O}_4/p\text{-RuNP}$ nanocatalyst (80 mg/L).

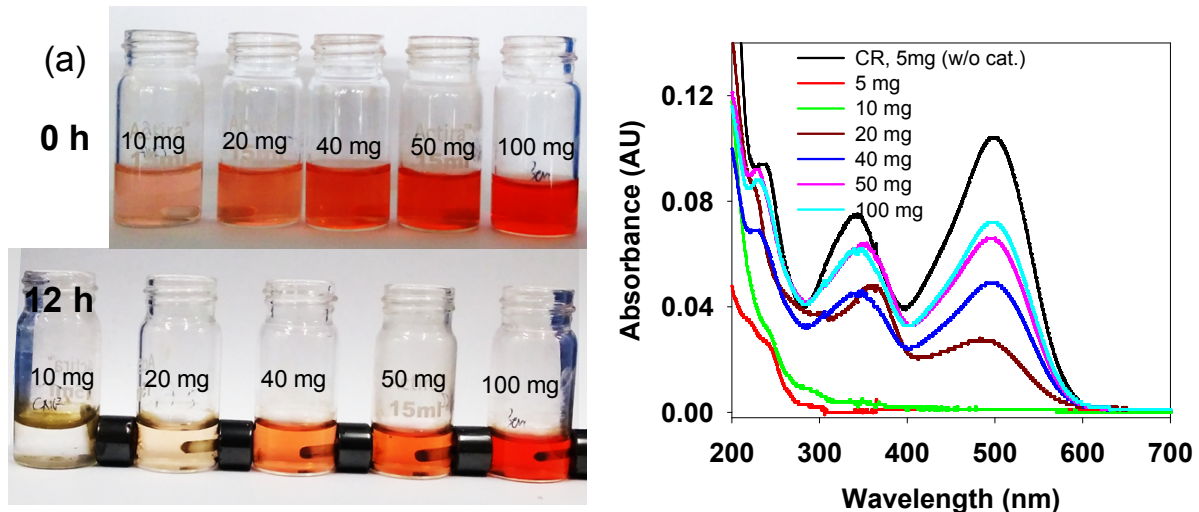


Figure S8. Photograph of CR dye of varying concentration (a) before and (b) after photodegradation (12 h) by $g\text{-C}_3\text{N}_4/\text{Fe}_3\text{O}_4/p\text{-RuNP}$ nanocomposite and (c) the corresponding UV-Vis spectra.

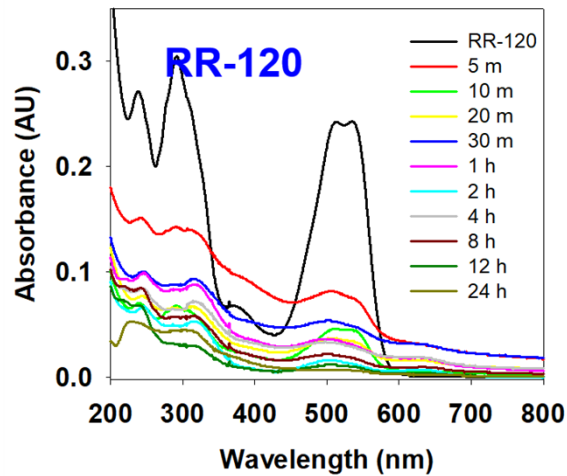
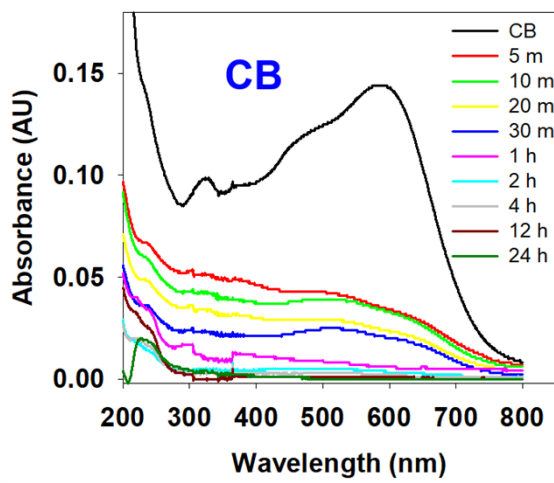
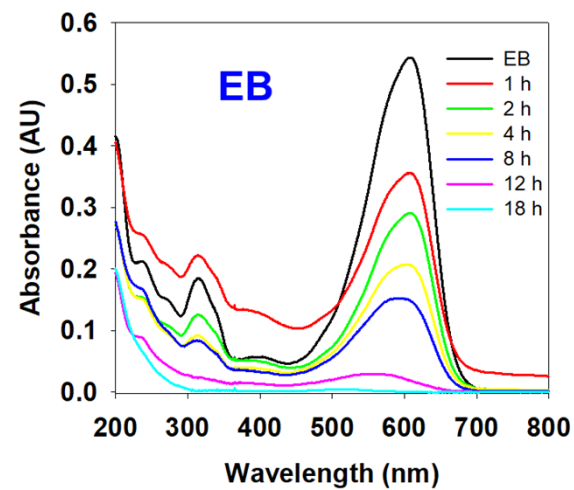


Figure S9. UV-Vis spectra of degradation of various azo dyes (5 mg/L) under LED in presence of $g\text{-C}_3\text{N}_4/\text{Fe}_3\text{O}_4/p\text{-RuNP}$ nanocatalyst (80 mg/L).

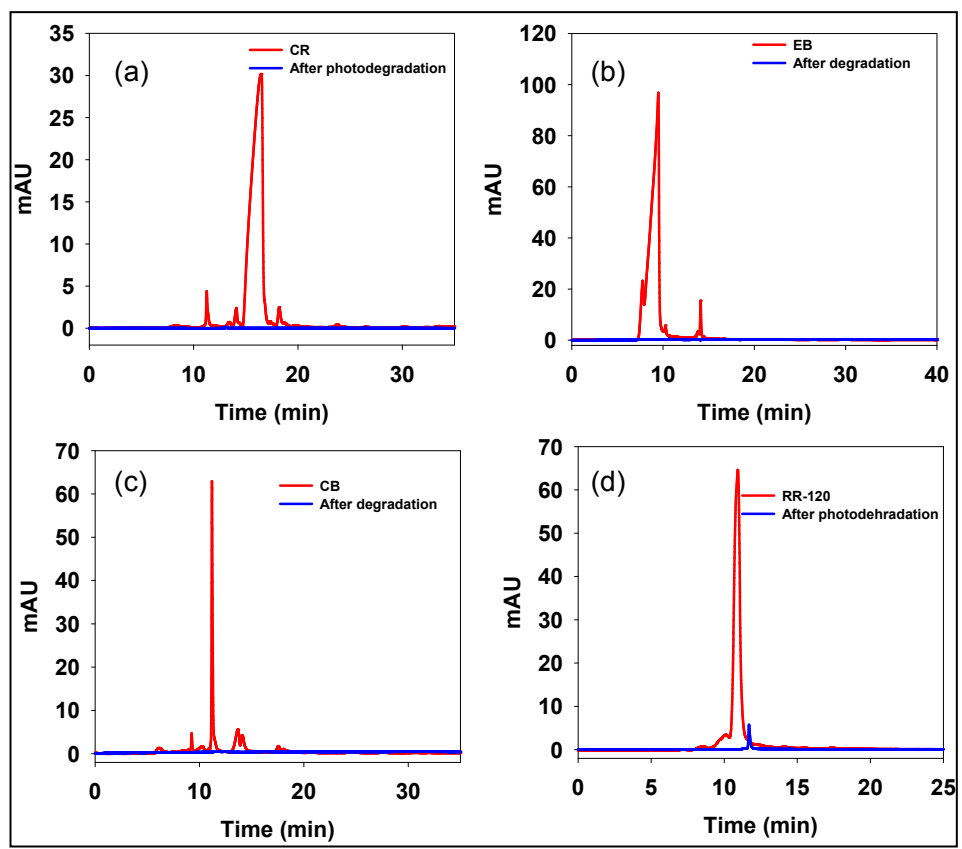


Figure S10. HPLC of azo-dyes (5 mg/L) after and before the degradation using visible light at pH 7.0 in presence of $g\text{-C}_3\text{N}_4/\text{Fe}_3\text{O}_4/p\text{-RuNP}$ (80 mg/L) nanocatalyst.

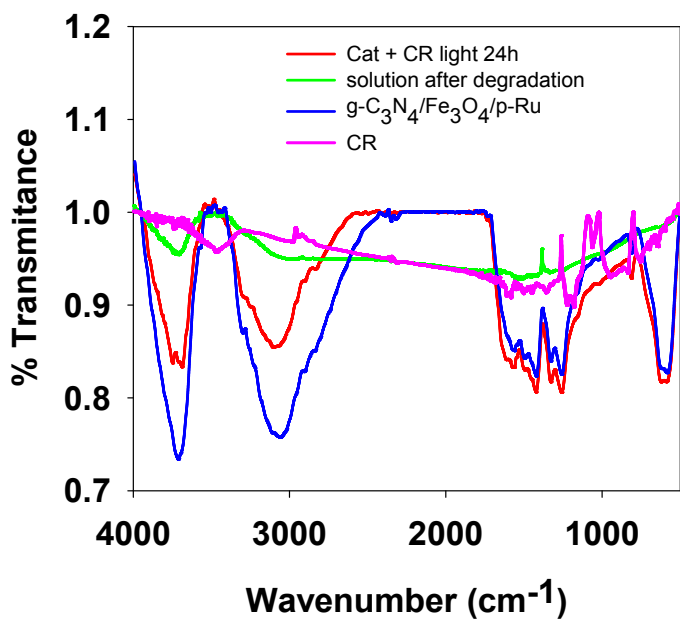


Figure S11. FTIR spectra of CR, $g\text{-C}_3\text{N}_4/\text{Fe}_3\text{O}_4/p\text{-Ru}$ NP nanocatalyst before and after photo-degradation of CR and the solution after complete degradation of CR.

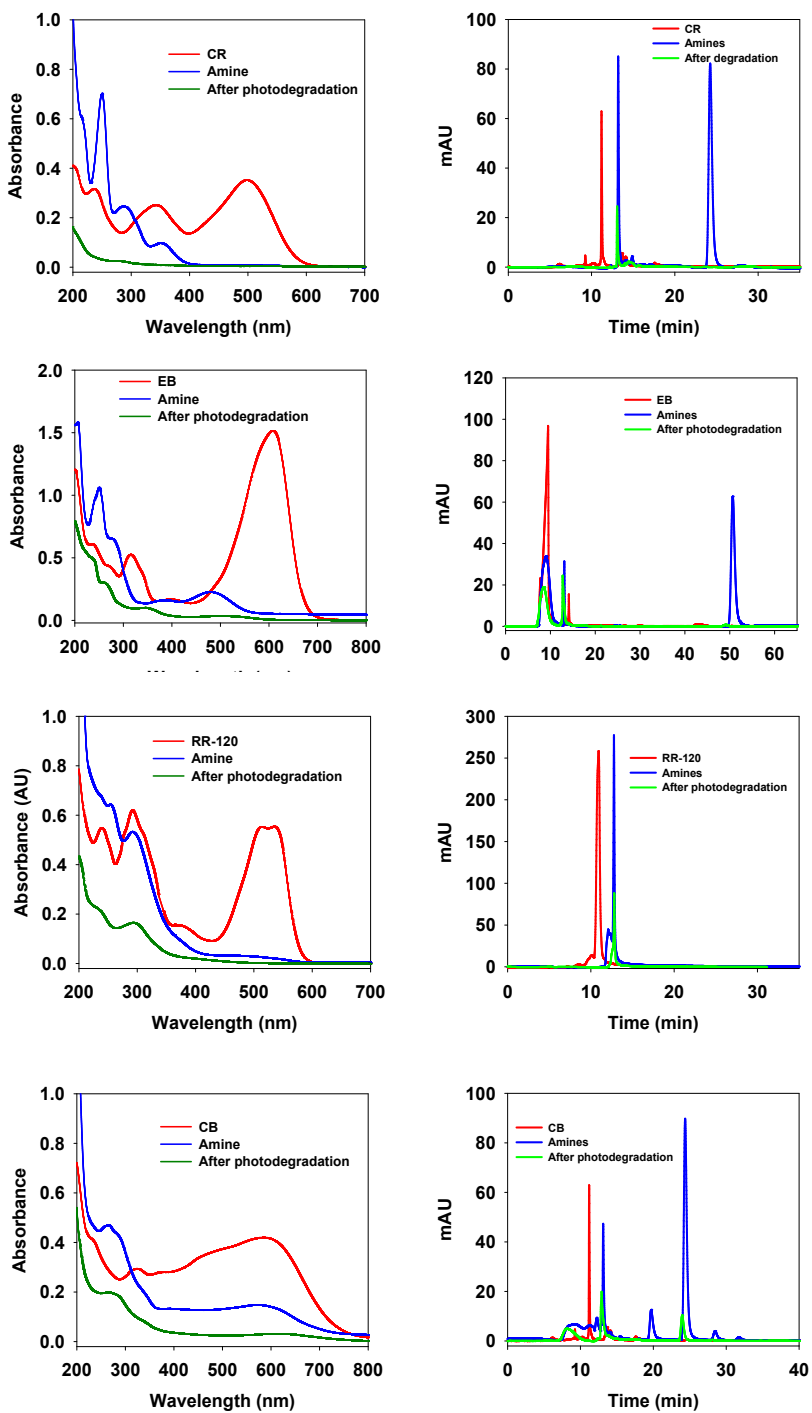


Figure S12. (a, c, e and g) UV-Vis spectra of azo dyes before (i), after(ii) reduction and after photo-degradation (iii); (b, d, f and h) HPLC of aromatic amines of reduced dyes (200 mg/L) after and before degradation using visible light at pH 7.0 in presence of $g\text{-C}_3\text{N}_4/\text{Fe}_3\text{O}_4/p\text{-RuNP}$ nanocatalyst (80 mg/L).

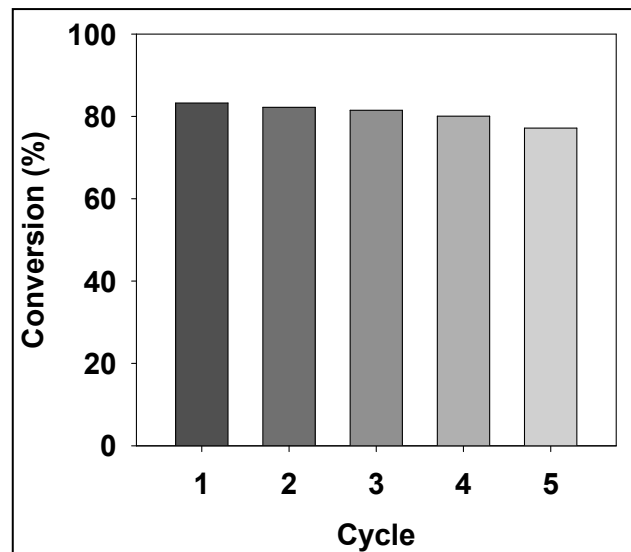


Figure S13. Reusability of $g\text{-C}_3\text{N}_4/\text{Fe}_3\text{O}_4/p\text{-RuNP}$ nanocatalyst towards aniline (100 mg/L) degradation under visible (LED) light.

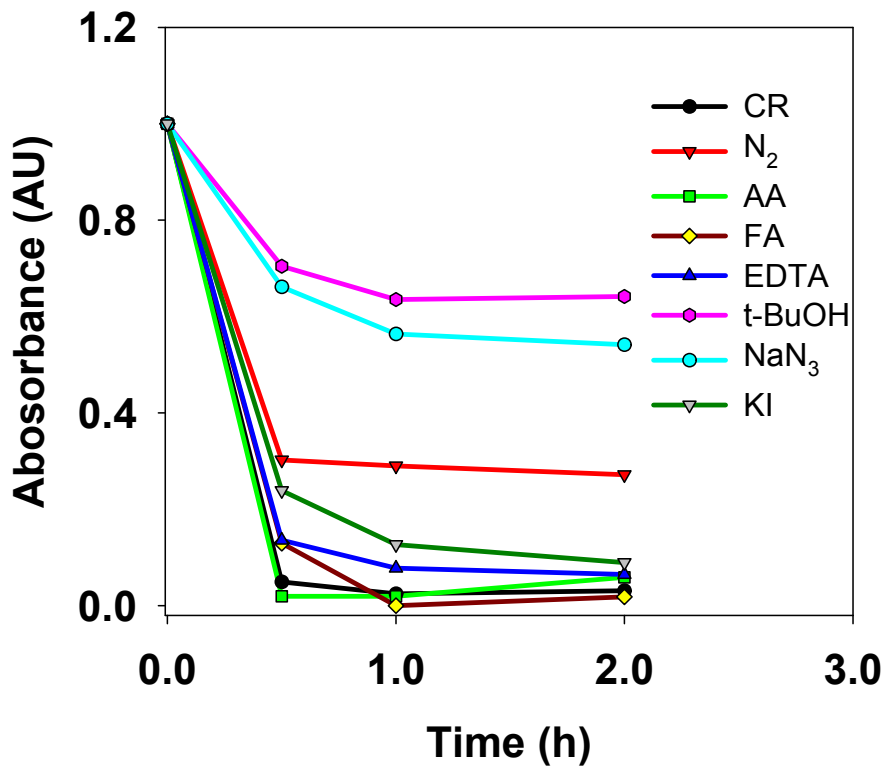


Figure S14. (a) UV-Vis spectra of congo red (CR) after treatment of $g\text{-C}_3\text{N}_4/\text{Fe}_3\text{O}_4/p\text{-RuNP}$ nanocatalyst in the presence of different radical scavengers under LED light.

References:

- 1 I. Casero, D. Sicilia, S. Rubio and D. Pérez-Bendito, *Water Res.*, 1997, **31**, 1985–1995.
- 2 V. López-Grimau, M. Riera-Torres, M. López-Mesas and C. Gutiérrez-Bouzán, *Color. Technol.*, 2013, **129**, 267–273.
- 3 A. Kumar Verma, P. Bhunia, A. K. Verma and R. R. Dash, *Adv. Environ. Res.*, 2014, **3**, 293–306.
- 4 A. M. Klibanov and E. D. Morris, *Enzyme Microb. Technol.*, 1981, **3**, 119–122.
- 5 E. Yilmaz, S. Memon and M. Yilmaz, *J. Hazard. Mater.*, 2010, **174**, 592–597.
- 6 E. Akceylan, M. Bahadir and M. Yilmaz, *J. Hazard. Mater.*, 2009, **162**, 960–966.
- 7 A. Sahoo, S. K. Tripathy, N. Dehury and S. Patra, *J. Mater. Chem. A*, 2015, **3**, 19376–19383.
- 8 A. Sahoo and S. Patra, *ACS Appl. Nano Mater.*, 2018, **1**, 5169–5178.